physics

MDPI

*Article*

# 3D–2D Crossover and Phase Shift of Beats of Quantum Oscillations of Interlayer Magnetoresistance in Quasi-2D Metals

**Taras I. Mogilyuk [1], Pavel D. Grigoriev [2,3,4,*], Vladislav D. Kochev [3], Ivan S. Volokhov [1,3,5] and Ilya Y. Polishchuk [1,6]**

1 Department of Condensed Matter, National Research Center (NRC) Kurchatov Institute, Kurchatov Square 1, Moscow 123182, Russia
2 L.D. Landau Institute for Theoretical Physics of the Russian Academy of Sciences, Akad. Semenov Avenue 1a, Chernogolovka 142432, Russia
3 Department of Theoretical Physics and Quantum Technology, National University of Science and Technology (NUST)—"MISIS", Leninskiy Avenue 4, Moscow 119049, Russia
4 Kotelnikov Institute of Radioengineering and Electronics of the Russian Academy of Sciences, Mokhovaya 11-7, Moscow 125009, Russia
5 Lebedev Physical Institute of the Russian Academy of Sciences, Leninsky Avenue 53, Moscow 119991, Russia
6 Theoretical Physics Department, Moscow Institute for Physics and Technology (MIPT), Institutskiy Per. 9, Dolgoprudny 141701, Russia
* Correspondence: grigoriev@itp.ac.ru

**Abstract:** Magnetic quantum oscillations (MQOs) are traditionally applied to investigate the electronic structure of metals. In layered quasi-two-dimensional (Q2D) materials, the MQOs have several qualitative features, offering additional helpful information, provided their theoretical description is developed. Within the framework of the Kubo formula and the self-consistent Born approximation, we reconsider the phase of the beats in the amplitude of the Shubnikov oscillations of the interlayer conductivity in Q2D metals. We show that the phase shift of the beats of the Shubnikov (conductivity) oscillations relative to the de Haas–van Alphen (magnetization) oscillations is larger than woud be expected and, under certain conditions, can reach the value of $\pi/2$, as observed experimentally. We explain the phase inversion of the MQOs during the 3D–2D crossover and predict the decrease in the relative MQO amplitude of the interlayer magnetoresistance in a strong magnetic field, larger than the beat frequency.

**Keywords:** quasi-two-dimensional metals; layered materials; quantum magnetization; interlayer conductivity; magnetic quantum oscillations; beating phase



**Citation:** Mogilyuk, T.I.; Grigoriev, P.D.; Kochev, V.D.; Volokhov, I.S.; Polishchuk, I.Y. 3D–2D Crossover and Phase Shift of Beats of Quantum Oscillations of Interlayer Magnetoresistance in Quasi-2D Metals. *Physics* **2024**, *6*, 999–1012. https://doi.org/10.3390/physics6030061

Received: 18 April 2024
Revised: 17 June 2024
Accepted: 24 June 2024
Published: 25 July 2024



## 1. Introduction

Layered quasi-two-dimensional (Q2D) metals (see Figure 1) represent a wide class of materials, intermediate between the various 2D electron systems and usual three-dimensional (3D) compounds. The Q2D materials attract enormous research interest due to the variety of new electronic phenomena and diverse potential applications. They include high-temperature superconductors, organic metals, van der Waals crystals, artificial heterostructures, and so on. An experimental study of their electronic structure, in addition to ab initio calculations, is crucial for understanding and utilizing their properties. Although angle-resolved photoemission spectroscopy (ARPES) provides visual data on the electronic bands and Fermi surface (FS), more traditional tools, such as magnetic quantum oscillations (MQOs) [1], commonly have higher accuracy and availability.

The MQOs originate from the Landau-level (LL) quantization of the electron spectrum in a magnetic field field $\boldsymbol{B}$ and appear in all thermodynamic and transport quantities as their periodic $1/B$ dependence. The standard MQO theory, based on the Lifshitz–Kosevich (LK) formula [2] (see [1] for modern LK theory), is often applied even in Q2D metals and provides the FS extremal cross-section areas $S_i = 2\pi e\hbar F_i/c$ from the fundamental MQO

frequencies, $F_i$, with $e$ denoting the elementary charge, $c$ the speed of light, and $\hbar$ the reduced Planck constant. Such data, collected at various directions of the magnetic field $\boldsymbol{B}$, helped to determine the FS of most known metals. Less accurate, the LK theory also describes the damping of the MQO amplitude by temperature and disorder as a function of the magnetic field strength $\boldsymbol{B}$, which enables estimating the electron effective mass and mean free time for each band [1].

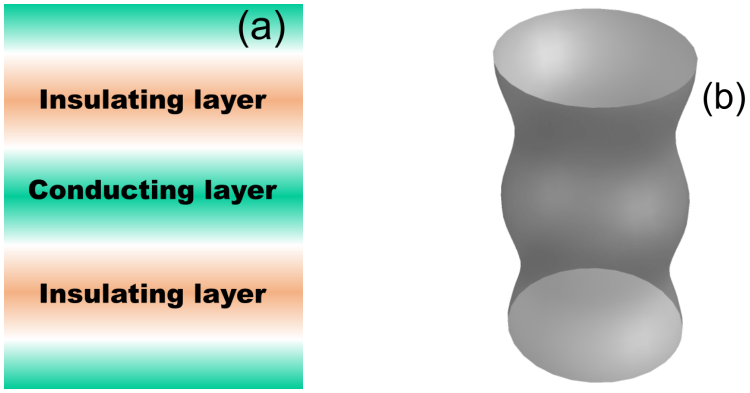


**Figure 1.** Schematic representation of a layered Q2D metal (**a**) and its Fermi surface (**b**).

The strong anisotropy of layered Q2D metals introduces special features to MQOs. The Q2D electron dispersion, obtained in the tight-binding approximation for the interlayer $z$ direction, is provided by

$$\epsilon_{3D}(\boldsymbol{k}) = \epsilon_{\|}\left(\boldsymbol{k}_{\|}\right) - 2t_z \cos(k_z d), \tag{1}$$

where $\boldsymbol{k}$ denotes the wavenumber, $\epsilon_{\|}\left(\boldsymbol{k}_{\|}\right)$ is the intralayer electron dispersion, $t_z$ is the interlayer transfer integral of electrons, and $d$ is the lattice constant along the $z$-axis. Often, in Q2D metals, the Fermi energy $\mu \gg t_z$, and the FS is a warped cylinder with two close cross-section areas corresponding to the "neck" and "belly" of the FS (see Figure 1b). According to the LK theory, at $\boldsymbol{B}$ parallel $z$, the MQOs have two close fundamental frequencies $F_1 = F - \Delta F/2$ and $F_2 = F + \Delta F/2$. As the MQO amplitudes with these two frequencies are also close, the resulting MQOs at frequency $F$ have amplitude modulations with frequency $\Delta F$, called beats. The beat frequency $\Delta F$ is proportional to the interlayer transfer integral: $\Delta F/F \approx 4t_z/\mu$. It non-monotonously depends on the direction of the magnetic field, which follows the angular magnetoresistance oscillations (AMROs) [3–6], and can be used to determine the in-plane Fermi momentum [5,6] and even high harmonics of FS warping [7,8].

Even if the MQOs are weak, the interlayer electron transport in Q2D metals exhibits several unique properties, such as the aforementioned AMROs [3–6] and longitudinal interlayer magnetoresistance [9–11]. There are even more new features of MQOs in Q2D metals that are not described within the standard LK theory. The interplay between the angular and quantum magnetoresistance oscillations is nontrivial [12,13] and leads to the angular modulations of the MQO amplitude [13]. The so-called difference or slow oscillations (SOs) of magnetoresistance [14–17] at frequency $2\Delta F$ appear and survive at much higher temperatures than the usual MQOs. The SOs help to determine the type of disorder and provide further practical information, such as the interlayer transfer integral. Another feature beyond the LK theory is the phase shift of the beats between the MQOs of the thermodynamic and transport quantities [15,18]. This phase shift increases with $B$, as observed in various Q2D metals [18–20] and substantiated theoretically [15,18]. The experimentally observed phase shift of the beats $\Delta\phi_{\text{exp}}$ often considerably exceeds the theoretical prediction $\Delta\phi_{\text{theor}}$ (e.g., see Figure 3 in Ref. [15] or Figure 6 in Ref. [19]). In the present paper, we explain this inconsistency and develop a more accurate theory of this effect.

The beatings of the MQO amplitude due to the interlayer electron hopping were observed in a number of other layered materials [5,6,21–25]. Note that the phase shift of the beats is observed not only between the de Haas–van Alphen (dHvA) and the Shubnikov–de Haas (SdH) effects but also between the oscillations of other quantities, e.g., the interlayer magnetoresistance and thermopower [22], or magnetoresistance and specific heat [26]. The MQOs of magnetization and of the interlayer conductivity were also measured simultaneously in the Dirac semimetals $BaGa_2$ [27]. There are various other combined SdH and dHvA measurements in layered metals where the MQO beats are observed [28–31]. Similar beating effects may also appear in artificial heterostructures and multilayer topological insulators [32,33], as well as in layered Weyl semimetals [26].

Another noticeable feature of the 3D–2D crossover, driven by the parameter $\lambda = 4\Delta F/B_z$ (where $B_z$ denotes the magnetic field component along the $z$-axis), is the phase inversion of the MQOs of conductivity as compared to those of the electronic density of state (DoS) at the Fermi level and, hence, of all the thermodynamic quantities. At a considerably low magnetic field, the MQOs of conductivity and DoS have opposite phases as soon as the former is proportional to the electron mean free time, which is inversely proportional to the DoS [34,35], according to the golden Fermi rule or the Born approximation. However, in a high magnetic field $B_z \gg \Delta F$ in Q2D metals, when the Landau levels (LLs) become separated and the DoS between the LLs is zero, the MQO phase of conductivity and DoS coincide. The latter follows both from the direct observations [10,36,37] and calculations [9–11,17,38], being supported by the simple qualitative argument that if the DoS at the Fermi level is zero the conductivity must also be zero at a low temperature. However, in spite of a general understanding, the quantitative description of this phase inversion is absent. In Section 4, we show how this phase inversion during the 3D–2D crossover is described by analytical formulas. The understanding of this MQO phase inversion is helpful for experimental studies of the Berry phase using MQO measurements [39–42].

## 2. Available Experimental Observations and Their Description

The MQOs have been extensively investigated in various Q2D metals, including the cuprate [43–46] and iron-based [47,48] high-$T_c$ superconductors, organic metals [5,6], van der Walls layered crystals, artificial heterostructures, and various of other materials. The two most common MQO experiments are the measurements of magnetization and conductivity oscillations, i.e., the dHvA and the SdH effects. However, the observation of the phase shift between their beats is less common because it requires the measurements of both these effects on the same sample.

In Ref. [19], the Fermi surface of a layered organic metal (BEDT-TTF)$_4$[Ni(dto)$_2$] was studied by measuring the quantum oscillations of both magnetization and interlayer conductivity. The authors have shown that the standard LK theory [1] quite well describes the results on magnetization oscillations. The detected positions of the beat nodes of the dHvA oscillation amplitude are quite well fitted by the formula

$$B_{\text{node}} = \frac{4}{4N_{\text{node}} - 1}\Delta F,\ N_{\text{node}} = 1,\ 2,\ 3, \ldots, \tag{2}$$

where $\Delta F$ is the beat frequency providing the FS warping. However, the observed positions of the beat nodes of the Shubnikov oscillation amplitude in Ref. [19] are found to be considerably shifted and well enough fitted by another formula:

$$B_{\text{node}} = \frac{4}{4N_{\text{node}} + 1}\Delta F,\ N_{\text{node}} = 0,\ 1,\ 2,\ 3, \ldots . \tag{3}$$

A similar difference in the positions of the beat nodes of dHvA oscillations and Shubnikov oscillations was also observed in $\kappa$-(BEDT-TTF)$_2$Cu[N(CN)$_2$]Br [20]. The LK theory does not explain the observed phase shift of the beat nodes regarding $\pi/2$ between the oscillations of magnetization and interlayer conductivity.

The 3D–2D crossover in the MQO behavior happens [10] when $B \sim \Delta F$, i.e., when the LL separation $\hbar\omega_c$ becomes comparable to the interlayer bandwidth $4t_z$, where $\omega_c = eB/(m^*c)$ is the cyclotron frequency, with $m^*$ the effective electron mass. The phase shift between the MQO beats of dHvA and SdH effects is considerable when $\hbar\omega_c \gtrsim 4t_z$, i.e., during this 3D–2D crossover.

The expressions for interlayer conductivity derived [14,18] in the tau approximation highly underestimate the observed phase shift $\phi_b$ between the beats of magnetization and interlayer conductivity, providing

$$\phi_b = \arctan[\hbar\omega_c/(2\pi t_z)], \tag{4}$$

Equation (4) always predicts $\phi_b < \pi/2$, which does not explain the experimental data from Ref. [19]. Note that the phase shift of the beats observed in Ref. [18] is also about 2.4 times larger than the prediction of Equation (4). Indeed, substituting the known parameters in the Q2D organic metal $\beta$-(BEDT-TTF)$_2$IBr$_2$, namely the cyclotron mass $m^* = 4.2m_e$, with $m_e$ the electron mass, as obtained from the temperature dependence of the MQO amplitude, and the interlayer bandwidth $4t_z = 1.15$ meV, as extracted from the ratio between the beating and fundamental MQO frequencies, into Equation (4), one obtains the 2.4 times smaller slope of the linear dependence of $\tan\phi_b$ on $B_z$ than the experimental data in Figure 4 from Ref. [18].

The calculations of the interlayer conductivity using the Kubo formula predict a larger phase shift of the beats provided by [15]

$$\tan\phi_b = \frac{\hbar\omega_c}{2\pi t_z}\left(1 + \frac{2\pi^2 k_B T_D}{\hbar\omega_c}\right) = \frac{\hbar\omega_c}{2\pi t_z}\left(1 + \frac{\pi}{\omega_c\tau}\right) \equiv \frac{\hbar\omega_c}{2\pi t_z}(1+\gamma_0), \tag{5}$$

where $T_D \equiv \hbar/(2\pi k_B\tau)$ is called the Dingle temperature, $k_B$ is the Boltzmann constant, $\tau$ is the electron mean free time, and $\gamma_0 = \pi/(\omega_c\tau)$ is the dimensionless parameter. MQO damping by crystal disorder. These quantities enter the Dingle factor $R_{D0} = \exp(-\gamma_0) = \exp[-2\pi^2 k_B T_D/(\hbar\omega_c)]$, describing the damping of MQOs by crystal disorder (see Equations (6)–(8) below). However, even this enhanced phase shift of the beats provided by Equation (5) is still insufficient to quantitatively describe the effect observed in Refs. [18,19].

Note that $\tau$ measured from the MQOs is, generally, shorter than the transport mean free time $\tau_{tr}$ and the mean free time, $\tau^*$, arising from short-range disorder only and measured from the damping of slow magnetoresistance oscillations [14]. This difference, $\tau < \tau^* \approx \tau_{tr}$, appears because the MQOs are damped not only by short-range disorder but also by long-range sample inhomogeneities, which smear the Fermi energy similar to the temperature effect [10,14–17]. The opposite case when the transport mean free time $\tau_{tr} < \tau \lesssim \tau^*$ is also possible in heterogeneous conductors, where there are rare but strong inhomogeneities, such as domain walls or linear crystal defects. Then, inside each domain of the size larger than the Larmor radius, the material is a clean metal with a large $\tau{\sim}\tau^*$, but the electronic transport across the sample is complicated due to of its heterogeneity, which corresponds to quite a short time $\tau_{tr}$. As follows from the calculations in Refs. [15,17], it is $\tau^*$ rather than $\tau$ that enters Equation (5).

## 3. Analysis Input

The materials to which our study is applicable are the strongly anisotropic layered Q2D metals, where $t_z$ is of the same order of magnitude as $\hbar\omega_c$. For the comparison of our formulas with experiments, we take the data from Refs. [18,19] obtained on the organic metals (BEDT-TTF)$_4$[Ni(dto)$_2$] and $\beta$-(BEDT-TTF)$_2$IBr$_2$.

Throughout this study, we consider $\boldsymbol{B}$ perpendicular to conducting layers, so that $B = B_z$. We use the expressions for the MQOs of magnetization and interlayer conductivity from Refs. [15,17,49,50] obtained in the self-consistent Born approximation. In the leading

order of the expansion in powers of the Dingle factor $R_{D0}$ at temperature $T$, the oscillating part of the magnetization reads (see Equation (33) in Ref. [49] or Equation (6) in Ref. [50])

$$\widetilde{M} \approx \frac{e\mu}{2\pi^2\hbar cd} R_{D0} R_T \left[ J_0(\lambda)\sin(\overline{\alpha}) + \frac{\lambda}{\overline{\alpha}} J_1(\lambda)\cos(\overline{\alpha}) \right], \tag{6}$$

and the oscillating part of the interlayer conductivity is (see Equation (18) in Ref. [15] or Equation (64) in Ref. [17])

$$\sigma_{zz}^{QO} \approx 2\overline{\sigma}_{zz}^{(0)} \cos(\overline{\alpha}) R_{D0} R_T R_{z\sigma}, \;\; R_{z\sigma} = J_0(\lambda) - \frac{2}{\lambda}(1+\gamma_0) J_1(\lambda), \tag{7}$$

where $\lambda = 4\Delta F/B_z = 4\pi t_z/(\hbar\omega_c)$, $\overline{\alpha} = 2\pi\mu/(\hbar\omega_c)$, $J_0$ and $J_1$ are the Bessel functions of zero and first orders, respectively, $\overline{\sigma}_{zz}^{(0)}$ is the interlayer conductivity without magnetic field, and $R_T = 2\pi^2 k_B T/(\hbar\omega_c)/\sinh(2\pi^2 k_B T/(\hbar\omega_c))$ is the temperature damping factor of MQOs.

At strong Q2D anisotropy, when $2t_z/\mu = \lambda/\overline{\alpha} \ll 1$ and the beats of MQOs are the most pronounced, the last term in the square brackets of Equation (6) can be omitted, and the oscillating part of magnetization simplifies to

$$\widetilde{M} \approx \frac{e\mu}{2\pi^2\hbar cd} \sin(\overline{\alpha}) R_{D0} R_T R_M, \;\; R_M = J_0(\lambda). \tag{8}$$

The MQOs correspond to the rapidly oscillating factors $\sin(\overline{\alpha})$ or $\cos(\overline{\alpha})$ in Equations (6)–(8), while the factors $R_M$ and $R_{z\sigma}$ describe the beats of the MQO amplitudes and are the subject of our study.

## 4. Analysis and Results

Let us first consider the limit of $\lambda \gg 1$, corresponding to a rather large electron interlayer transfer integral $4\pi t_z \gg \hbar\omega_c$ or weak magnetic field. Then, one can use the large-argument asymptotic expansions of the Bessel functions in Equations (7) and (8). As a result, the beating factors of the MQO amplitudes in Equations (7) and (8) simplify to

$$R_M = \frac{\sqrt{2/\pi}\cos(\lambda - \pi/4)}{\sqrt{\lambda}}, \tag{9}$$

$$R_{z\sigma} = \frac{\sqrt{2/\pi}\cos(\lambda - \pi/4)}{\sqrt{\lambda}} + \frac{(16\gamma_0 + 15)\cos(\lambda + \pi/4)}{4\sqrt{2\pi}\lambda^{3/2}}. \tag{10}$$

At $\lambda \gg 2(\gamma_0 + 1)$, the second term in Equation (10) is negligibly small, and one obtains the same beating factors of the MQOs of magnetization and interlayer conductivity,

$$R_{z\sigma} \approx \frac{\sqrt{2/\pi}\cos(\lambda - \pi/4)}{\sqrt{\lambda}} = R_M. \tag{11}$$

Hence, in this limit, the phase shift of the beats is absent: $\phi_b \approx 0$.

In the opposite limit of strong MQO damping by disorder, $\gamma_0 \gg \lambda/2$, the first term in Equation (10) can be omitted, and one obtains

$$R_{z\sigma} \approx \frac{2^{3/2}\gamma_0 \cos(\lambda + \pi/4)}{\sqrt{\pi}\lambda^{3/2}}. \tag{12}$$

Comparing Equations (9) and (12), one can see that, at $\gamma_0 \gg \lambda/2$, the MQO beats of the interlayer conductivity are shifted from those of magnetization by the phase $\phi_b = \pi/2$. As follows from Equation (9), the beat nodes of magnetization oscillations $\widetilde{M}$ in Equation (8) are located at $\lambda \approx -\pi/4 + \pi N_{node}$, where $N_{node} \geq 1$ is an integer, and from Equation (12) it follows that the beat nodes of the interlayer conductivity oscillations $\sigma_{zz}^{QO}$ provided by Equation (7) are shifted by $\pi/2$ and located at $\lambda \approx \pi/4 + \pi N_{node}$. These $\lambda$ values

provide the same position of the beat nodes as the expressions (2) and (3) for $N_{\rm node} \geq 1$ and $\Delta F = \lambda|B_z|/\pi$, corresponding to the fit of the experimental data in Ref. [19]. Hence, Equations (9) and (12) describe the experimental observations in Ref. [19] quite well. However, Equation (12) assumes $\gamma_0 \gg \lambda/2$, while $\gamma_0 \sim \lambda$ in the experiment in Ref. [19]. The Dingle temperature extracted from the experimental data in Ref. [19] is $T_{\rm D} \approx 0.5$ K. The beat frequency in the organic metal (BEDT-TTF)$_4$[Ni(dto)$_2$] studied in Ref. [19] is $\Delta F \approx 4.5$ T, which corresponds to $t_z = 0.06$ meV $\approx 0.7$ K. Hence, the ratio $\gamma_0/\lambda = 2\pi^2 T_{\rm D}/(4\pi t_z) = \pi T_{\rm D}/(2t_z) \approx 1.12$ in Ref. [19]. Then, to improve the quantitative description of the observed phase shift of the MQO beats, one needs to consider the case $\lambda \sim \gamma_0 \sim 1$ more carefully.

The phase shift $\phi_{\rm b}$ of the MQO beats becomes even stronger than that provided by Equations (9) and (12) if one applies Equations (7) and (8) without the asymptotic expansions of the Bessel functions at a large argument, i.e., without the assumption $\lambda \gg 1$, which is more relevant to the experiment in Ref. [19]. In Figure 2, using Equations (7) and (8) at $\gamma_0(\lambda) = \{0.1, 1.12, 2, 3\}\lambda$, we plot the beating factors $R_M$ and $R_{z\sigma}$, describing the MQO amplitudes of magnetization and conductivity without the Dingle and temperature damping factors. The theoretical curves in Figure 2 correspond to four values $\gamma_0/\lambda = \{0.1, 1.12, 2, 3\}$ to describe the experimental data from Refs. [18,19], where $\gamma_0/\lambda \approx 0.1$ and $\gamma_0/\lambda \approx 1.12$ correspondingly. In Figure 2, we take a special scale of the abscissa axis so that the zeros of both curves, called the beat nodes, fall into integer values. From Figure 2, one finds that the beat nodes for the interlayer conductivity oscillations $\sigma_{zz}^{\rm QO}$ (7) are shifted relative to the magnetization oscillating $\widetilde{M}$ (8) beat nodes by a quarter of the period $\lambda \approx \pi\Delta F/|B_z|$. (In Ref. [17], we used a different definition of $\Delta F \approx 2t_z B_z/(\hbar\omega_c) = \lambda B_z/\pi$.) The beat nodes of $\widetilde{M}$ in Figure 2 are located at $4\lambda/\pi \approx \{3, 7, 11, 15\}$. This coincides with the prediction of simplified limiting-case Formula (9) and remarkably well agrees with the experimental data from Ref. [19] fitted by Equation (2). At $\gamma_0(\lambda) = 0.1\lambda$, the positions of $\sigma_{zz}^{\rm QO}$ are close to the positions of the beat nodes of the amplitude of the magnetization oscillations. The beat nodes of $\sigma_{zz}^{\rm QO}$ plotted in Figure 2 at $\gamma_0(\lambda) = \{1.12, 2, 3\}\lambda$ are located at $4\lambda/\pi \approx \{0, 5, 9, 13\}$. For $N_{\rm node} \geq 1$, the positions coincide with Equation (3), which fits the experimental data from Ref. [19].

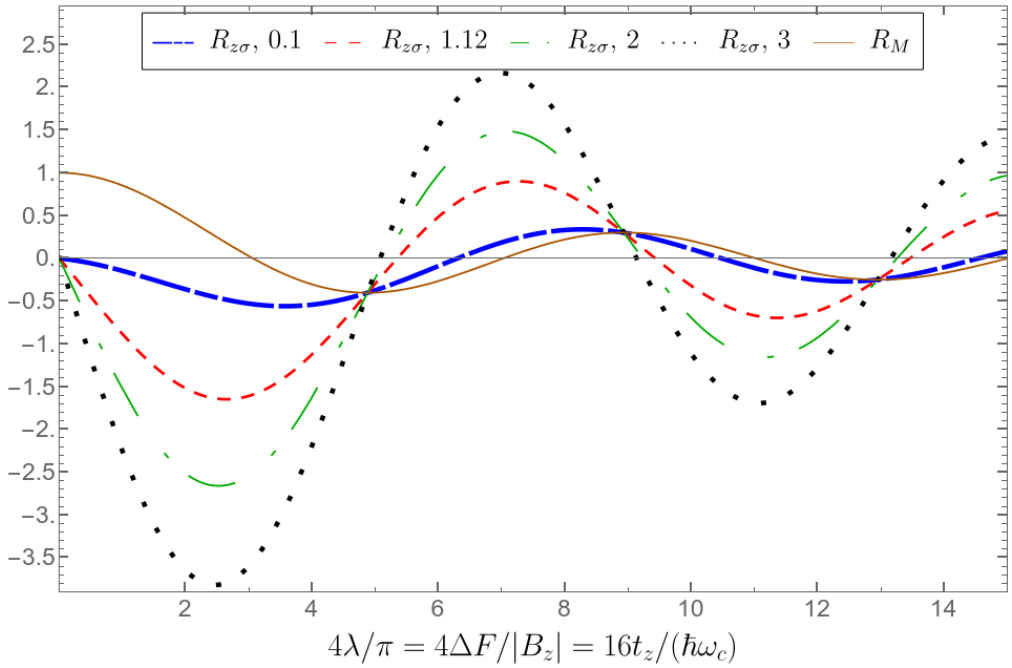


**Figure 2.** The beating factors $R_{z\sigma}$ (see Equation (7)) and $R_M$ (8) as functions of the inverse magnetic field, $1/|B_z|$. $R_{z\sigma}$ is shown for $\gamma_0/\lambda = 0.1$, 1.12, 2, and 3, as indicated.

Equations (7) and (8) also remarkably well agree with the experimental data from Ref. [18]. Figure 3 shows the measured positions of the magnetization and conductivity beat nodes from the experiments [18,19] along with the theoretical predictions by Equations (7) and (8). The measured positions of the beat nodes in Ref. [19] at $N_{\rm node} \geq 1$ are remarkably well described by Equations (2) and (3). Figure 3 demonstrates exceptionally good agreement between the theory developed here and the experimental data [18,19] for the beat-node positions with number $N_{\rm node} \geq 1$. These beat-node positions for the MQOs of magnetization and interlayer conductivity are fitted quite well by two straight lines each one parallel to another. Hence, one concludes that Equations (7) and (8) describe the beating nodes with $N_{\rm node} \geq 1$ remarkably well. Let us note that though the experimental data in Refs. [18,19] are taken on different compounds, they both show agreement with the proposed theory.

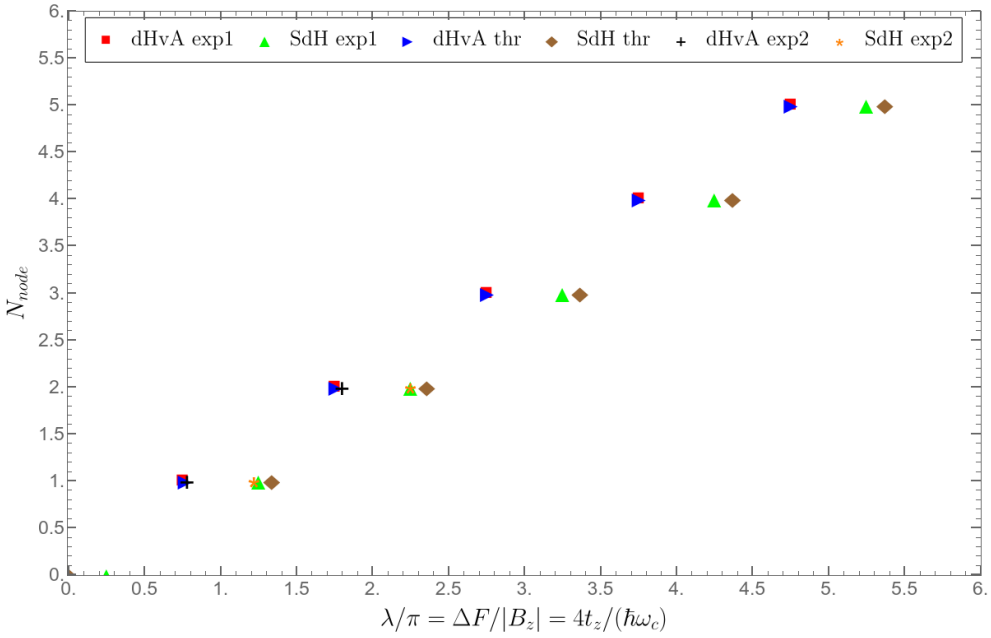


**Figure 3.** The dependence of the beat-node positions, $N_{\rm node}$, of the MQOs of $\sigma_{zz}^{\rm QO}$ and $\widetilde{M}$ on the inverse magnetic field, $1/|B_z|$, for $\gamma_0 = 1.12\lambda$. "dHvA exp1" and "SdH exp1" denote the experimental data from Ref. [19], relatively well fitted by expressions (2) and (3), "dHvA exp2" and "SdH exp2" denote the experimental data from Figures 2 and 3 from Ref. [18], "dHvA thr" denotes the results obtained from the zeros of expression (9), and "SdH thr" denotes the results obtained numerically from the solution of $R_{z\sigma} = 0$.

The position $\lambda = 0$ of the zeroth beating node provided by Equation (7) holds at any ratio $\gamma_0/\lambda$, as illustrated in Figure 2 and can be shown analytically. Indeed, in a very high magnetic field $\lambda \to 0$, the ratio $\gamma_0/\lambda = \hbar/(4\tau t_z) \to$ const, and the zeroth beating node is provided by

$$R_{z\sigma} = J_0(\lambda) - \frac{2}{\lambda}(1+\gamma_0)J_1(\lambda) \approx -\frac{\gamma_0}{\lambda}\lambda + \frac{(\gamma_0-1)}{8}\lambda^2 = 0. \tag{13}$$

$\lambda = 0$ is the root of Equation (13) forany ratio $\gamma_0/\lambda$. Another root, $\lambda = \sqrt{8\gamma_0/(\gamma_0-1)}$, is physically irrelevant as soon as it provides a value that is too large:

$$\lambda = \frac{1+\sqrt{1+32\gamma_0^2/\lambda^2}}{2\gamma_0/\lambda} > 2\sqrt{2}, \tag{14}$$

far beyond the limit $\lambda \ll 1$, where the expansion (13) holds.

The position of the very first beat node at $N_{\rm node} = 0$ differs in Equations (3) and (7). According to Equation (3), the beating node $N_{\rm node} = 0$ of $\sigma_{zz}^{\rm QO}$ oscillations to be at $4\lambda/\pi = 1$, which does not coincide with the positions $N_{\rm node} = \infty$ or $\lambda = 0$ of the zeroth beating node provided by Equation (7) and shown in Figure 2. As just shown (see Equation (14)), the origin of this difference is not a "wrong" choice of the parameter $\gamma_0/\lambda$ entering Equation (7).

Actually, the position $\lambda = \pi/4$ of the zeroth beating node $N_{\rm node} = 0$, predicted by the "fit" (3), has not been observed experimentally. The beat frequency in the organic metal (BEDT-TTF)$_4$[Ni(dto)$_2$] studied in Ref. [19] is $\Delta F \approx 4.5$ T. According to Equation (3), the zeroth beating node is at $B = 4\Delta F \approx 18$ T. In Ref. [19], the experimental data on the SdH oscillations in (BEDT-TTF)$_4$[Ni(dto)$_2$] are shown only up to $B = 6$ T in Figure 6 in Ref. [19], while the data up to $B = 28$ T are provided only for the dHvA oscillations in Figure 3 in Ref. [19]. In Figure 6.1 in Ref. [51], the SdH data up to $B = 28$ T are shown for the same organic metal (BEDT-TTF)$_4$[Ni(dto)$_2$], and no beating nodes are observed in the magnetic-field interval 4 T $< B <$ 28 T. A similar difference in the beat-node positions of the dHvA and Shubnikov oscillations in the $\kappa$-(BEDT-TTF)$_2$Cu[N(CN)$_2$]Br [20] was also detected by the non-observation of the SdH beat node in the magnetic-field interval 16 T $< B <$ 28 T. Hence, Equation (7) describes the available experimental data on the MQO beats of the interlayer conductivity exceptionally well.

In Ref. [18], the Dingle temperature extracted from the experimental data is $T_{\rm D} = 0.8$ K, but the Dingle temperature from the scattering by short-range disorder is $T_{\rm D}^{*} = 0.15$ K; see Figure 4 in Ref. [14]. The beat frequency $\Delta F \approx 40.9$ T in the organic metal $\beta$-(BEDT-TTF)$_2$IBr$_2$ studied in Ref. [18] is considerably larger than in (BEDT-TTF)$_4$[Ni(dto)$_2$] studied in Ref. [19]. It corresponds to $t_z = 1.15$ meV $\approx 13.3$ K and $\gamma_0/\lambda \approx 0.1$. For $\gamma_0 \ll \lambda/2^{3/2}$, the expression (10) for $R_{z\sigma}(\lambda)$ is approximately same as Equation (11). Since Equations (9) and (11) are similar, the latter means that the beat nodes for magnetization, $\widetilde{M}$, and conductivity, $\sigma_{zz}^{\rm QO}$, oscillations are close at this limit. In Figure 4, we show that the beat nodes found at $\gamma_0 = 0.1\lambda$ fit quite well with the experimental data on the position of the beat nodes from Figure 3 of Ref. [18]. The higher the $N_{\rm node}$ of the MQO beat nodes of the magnetization and interlayer conductivity, the shorter the distance between them.

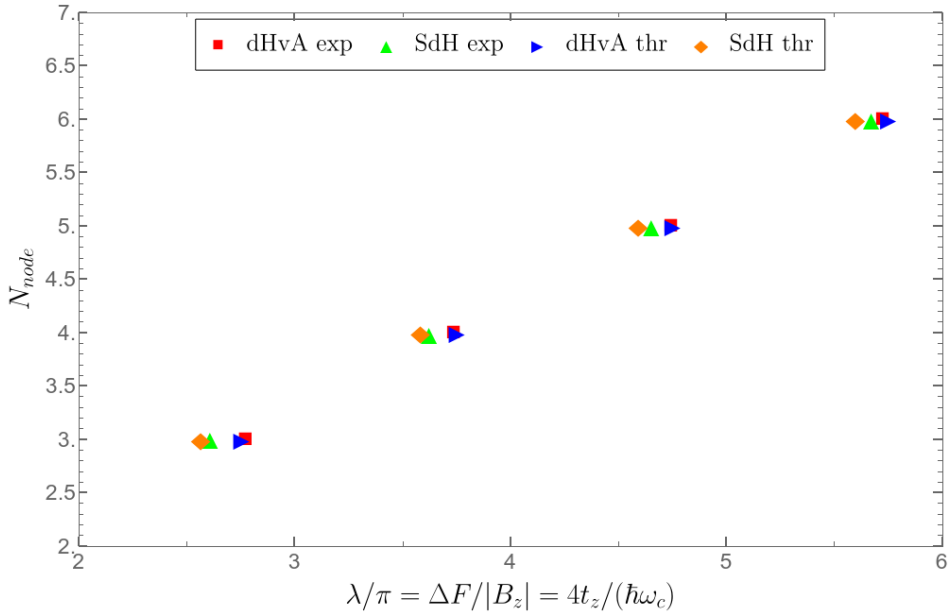


**Figure 4.** The dependence of the positions, $N_{\rm node}$, of the beat node of magnetic quantum oscillations of $\sigma_{zz}^{\rm QO}$ and $\widetilde{M}$ on the inverse magnetic field, $1/|B_z|$, for $\gamma_0(\lambda) = 0.1\lambda$. "dHvA exp" and "SdH exp" denote the measurements from Figure 3 in Ref. [18], "dHvA thr" denotes the results found from the zeros of expression (9), and "SdH thr" denotes those found from the numerical solution of $R_{z\sigma} = 0$.

## 5. Discussion

The analytical formulas obtained in this paper describe the interlayer conductivity $\sigma_{zz}$. These formulas can also be applied to describe the first MQO harmonic of the interlayer magnetoresistance $\rho_{zz} = 1/\sigma_{zz}$ if the MQOs are not strong enough so that the non-linear effects in the MQO amplitude may be neglected [52]. As soon as only the first MQO harmonic is kept and the higher-order terms in the MQO amplitude are negligible, one may safely apply the relation $\rho_{zz} = \sigma_{zz}^{-1}$ to describe the interlayer magnetoresistance [52]. However, for strong MQOs, their averaging over temperature and long-range disorder differs for $\rho_{zz}$ and $\sigma_{zz}$ [10,52].

A finite temperature $T$ suppresses the MQOs via the smearing of the Fermi energy by widening the Fermi–Dirac distribution function of the electrons, as provided by the damping factor $R_T$. This does not considerably affect the phases of MQOs and their beats. The second effect of raising the temperature is the enhancement of electron–electron (e–e) and electron–phonon (e–ph) interactions, which reduce the electron mean free time, $\tau(T)$. Although in the main order the effects of the e–e and e–ph interactions on the product of the Dingle and temperature damping factors $R_{\rm D}R_T$ cancel each other out [1,53–57], the phase shift of the beats provided by Equation (5) depends on $\tau$. Hence, with raising the temperature, a slight increase in the phase shift of the beats between the MQOs of the interlayer conductivity and magnetization may appear.

In this paper, we have shown that the developed theory and specifically Equation (7) describe quite well the available experimental data on the MQO beats of the interlayer conductivity $\sigma_{zz}$. They also predict some new remarkable and observable features. In particular, Equation (7) predicts a strong decrease in the MQO beating factor $R_{z\sigma}$ of the interlayer conductivity with the increase in the magnetic field, corresponding to $\lambda \to 0$. This decrease in $R_{z\sigma}$ is partially compensated by the Dingle factor $R_{\rm D0}$ and by the temperature damping factor $R_T$. However, the product $R_{\rm D0}R_TR_{z\sigma}$, describing the MQO amplitude of the interlayer conductivity, may still be non-monotonic in a high field, in contrast to the amplitude of the magnetization MQOs described by Equation (8), which always monotonically increases in a very high field at $\hbar\omega_c \gg t_z$. This nonmonotonic magnetic-field dependence of the MQO amplitude on the interlayer conductivity in a high field is rather robust to the variations in the material parameters, e.g, to the variations in temperature and sample quality provided by the ratio $\gamma_0/\lambda = \pi k_{\rm B}T_{\rm D}/(2t_z) = \hbar/(4t_z\tau)$. In Figure 5, we show this high-field non-monotonic dependence of the $\rho_{zz}$ MQO amplitude $(-1)R_{D0}R_TR_{z\sigma}$ on $\pi/\lambda = |B_z|/\Delta F$ for two different ratios $\gamma_0/\lambda$ and temperatures $T$. For all the sets of parameters, the MQO amplitude of the interlayer magnetoresistance in Figure 5 has a well seen maximum at $B_z^* \gtrsim 2\Delta F$ and decreases in a very high field $B_z > B_z^*$. At small ratios, $\gamma_0/\lambda < 0.3$, the increase in temperature up to the Dingle temperature, $T_{\rm D}$, has almost no effect on the graph, but, at higher $T \gtrsim t_z$, it shifts the MQO amplitude maximum at $B = B_z^*$ to higher fields, as shown in Figure 5. The exact value $B_z^*$ of the magnetic field where the MQO amplitude of the interlayer resistivity is maximal and starts to decrease depends on the electron mean free time $\tau$ and on the temperature, as one can see in Figure 5, as soon as (i) the MQO amplitude is the product of three damping factors according to Equation (7) and (ii) $R_{z\sigma}$ in Equations (7) or (13) contains $\gamma_0 \propto 1/\tau$, which determines the slope $\mathrm{d}R_{z\sigma}/\mathrm{d}\lambda$ at $\lambda \to 0$ and the maximal MQO amplitude of $\rho_{zz}$. This field $B_z^* \gtrsim 2\Delta F$ is rather large if $\Delta F \propto t_z$ is not quite small.

The predicted decrease in the MQO amplitude of the interlayer conductivity in a high field is somewhat counterintuitive, being the opposite to what is observed in magnetization, but it can be straightforwardly tested experimentally in various Q2D layered compounds, such as organic metals, van der Waals crystals, artificial heterostructures, and so on. We suppose that the proposed decrease in the MQO amplitude in a high field was actually observed in a number of experiments but mistaken for the non-existing beat node at a high magnetic field beyond the available range. For example, as mentioned in Section 4, in Refs. [19,20,51], the beating node $N_{\rm node} = 0$ of the SdH effect was not observed but assumed from some decrease in the MQO amplitude in a very high field. This decrease may

be considered as the experimental indication of the predicted high-field non-monotonic behavior of the MQO amplitude of the interlayer conductivity, but further experimental studies of this remarkable effect are required to be compared with the theoretical predictions made here and to determine the range of parameters where the effect is observed.

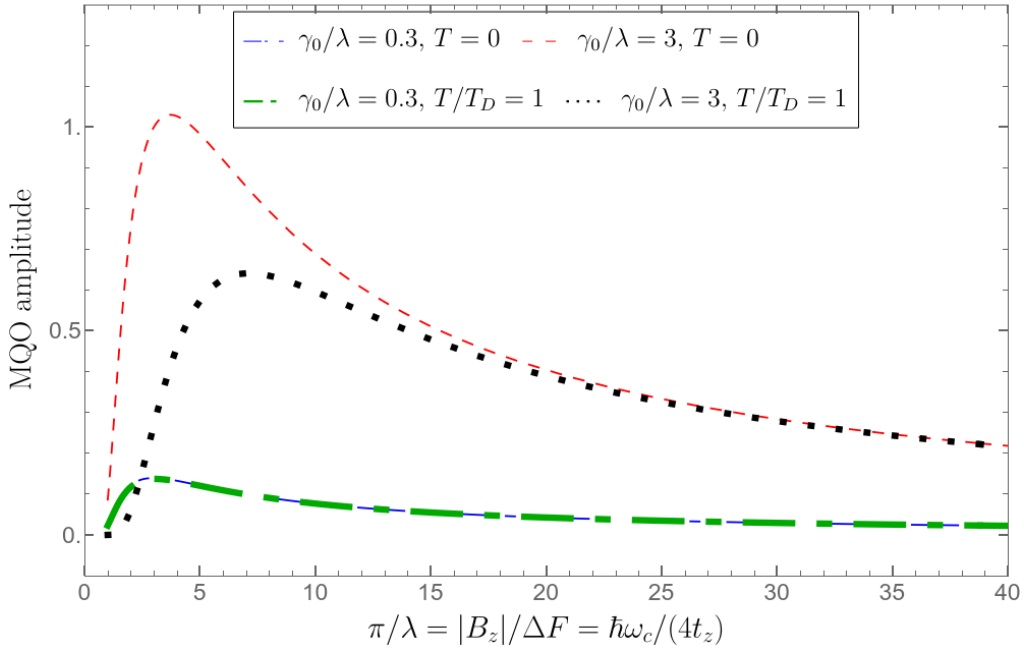


**Figure 5.** The MQO amplitude of interlayer conductivity $\sigma_{zz}$ in Equation (7) provided by the product $(-1)R_{D0}R_TR_{z\sigma}$ as a function of magnetic field for $\gamma_0 = \{0.3,\ 3\}\lambda$ at temperature $T = \{0,\ 1\}T_D$.

Another noticeable prediction of our theoretical analysis here is that all the curves in Figure 2, describing the MQO amplitudes, periodically cross at the same points. This can also be checked experimentally. However, this experimental test is less obvious and convenient than the above prediction of the monotonic magnetic-field dependence of the $\rho_{zz}$ MQO amplitude because the corresponding experimental data for the $M(B_z)$ and $R(B_z)$ magnetic oscillations must be properly normalized for such comparison.

Now, let us consider the MQO phase of the interlayer conductivity. For the Q2D electron spectrum (1) in a magnetic field, one can straightforwardly calculate [49,50], the one-particle DoS, $\nu$. Neglecting the higher harmonics, the DoS oscillations are provided by [49,50]

$$\widetilde{\nu} \approx \nu_0 2R_D R_\nu \cos(\overline{\alpha}),\ \ R_\nu = -J_0(\lambda), \tag{15}$$

where $\nu_0 = m_*/(2\pi\hbar^2 d)$ is its non-oscillating part per one spin component. The phase of DoS oscillations is strictly tied to that of magnetization provided by Equation (8) because the corresponding beating factors satisfy $R_\nu = -R_M$. In a weak magnetic field, when $\lambda \gg 1$ corresponding to the 3D limit, the second term in the beating factor $R_{z\sigma}$ of the interlayer conductivity provided by Equation (7) is much smaller than its first term. Then, $R_{z\sigma} \approx R_M = J_0(\lambda) = -R_\nu$, and the MQO phases of the interlayer conductivity $\sigma_{zz}$ and of the DoS $\nu$ are strictly opposite, as predicted by the 3D theory of the SdH effect [34,35]. In the opposite case, $\lambda < \pi$, corresponding to the 3D–2D crossover or nearly 2D limit, the SdH beating factor $R_{z\sigma} < 0$, as follows from Equation (7) and illustrated in Figure 5. Since $R_\nu = -R_M < 0$ is also negative at $\lambda < 1$, at the 3D–2D crossover $B \gtrsim \Delta F$ or in the almost 2D limit $B \gg \Delta F$, the quantum oscillations of the electronic DoS and of the interlayer conductivity have the same phase. One can see that our theory developed here describes the phase inversion of the SdH oscillations during the 3D–2D crossover.

The analysis presented here is generic to layered Q2D metals and can be applied to quite a wide class of layered compounds, which are still being actively studied by MQOs [25,27–30,58–61]. The dHvA effect measures a thermodynamic quantity, magneti-

zation, which only depends on the electron density of the states and its variations with the magnetic field. The SdH effect measures the electron transport and depends on the electron velocity and scattering time. The difference between the dHvA and SdH effects indicates the proximity to 3D–2D crossover, as shown in this paper. The comparative study provides additional knowledge about the electronic structure and scattering processes than the dHvA or SdH effects alone. For example, if the observed MQOs for some frequency are quite strong in terms of the SdH effect but much weaker or absent regarding dHvA, it is quite probable that these MQOs are difference-frequency oscillations or SO [14], and their frequency provides the interlayer bandwidth $4t_z$ or another energy splitting of the electronic spectrum rather than the area of the FS pockets.

## 6. Conclusions

In this paper, we developed the quantitative theoretical description of the beating phase of the magnetic quantum oscillations of the interlayer magnetoresistance and magnetization in Q2D metals, which are traditionally used to extract practical information about the electronic properties. The theory developed agrees remarkably well with the available experimental data and provides explanation for the long-standing puzzle of the observed exceptionally large phase shift of the beats between the MQOs of the thermodynamic and transport electronic properties. In addition, our theory also makes several new predictions that can be tested experimentally. The most unexpected prediction is the non-monotonic field dependence of the MQO amplitude of the interlayer magnetoresistance in a high magnetic field $B_z \sim \Delta F$, where $\Delta F$ is the beat frequency. Naively, one may expect a monotonic growth in the MQO amplitude of the interlayer conductivity in a strong magnetic field $|B_z| > \Delta F$, similar to magnetization, but we predict here its decrease at $|B_z| \gtrsim 4\Delta F$ in the regime of 3D–2D crossover, as illustrated in Figure 5. The analytical formulas obtained by us here also explain and describe the phase inversion of the SdH oscillations during the 3D–2D crossover.

**Author Contributions:** Conceptualization, P.D.G.; methodology, P.D.G. and T.I.M.; validation, I.S.V., V.D.K. and T.I.M.; formal analysis, T.I.M.; investigation, P.D.G. and T.I.M.; writing—original draft preparation, T.I.M.; writing—review and editing, P.D.G.; supervision, P.D.G.; funding acquisition, I.Y.P. and P.D.G. All authors have read and agreed to the published version of the manuscript.

**Funding:** This research was funded by the Russian Science Foundation grant #22-42-09018. V.D.K. acknowledges the Foundation for the Advancement of Theoretical Physics and Mathematics "Basis", Russia, for grant #22-1-1-24-1 and NUST "MISIS" grant No. K2-2022-025.

**Data Availability Statement:** Dataset available upon request from the authors.

**Conflicts of Interest:** The authors declare no conflicts of interest.

## Abbreviations

The following abbreviations are used in this manuscript:

| | |
|---|---|
| AMRO | angular magnetoresistance oscillations |
| ARPES | angle-resolved photoemission spectroscopy |
| BEDT-TTF | bis(ethylenedithio)tetrathiafulvalene |
| DoS | density of states |
| dHvA | de Haas–van Alphen |
| dto | dithiooxalate |
| FS | Fermi surface |
| LK | Lifshitz–Kosevich |
| LL | Landau level |
| MQO | Magnetic quantum oscillation |
| Q2D | quasi-two-dimensional |
| SdH | Shubnikov–de Haas |
| SO | slow oscillations |
| 2D, 3D | 2-, 3-dimensional |

## References


1. Shoenberg, D. *Magnetic Oscillations in Metals*; Cambridge University Press: Cambridge, UK, 1984. [CrossRef]
2. Lifshitz, I.M.; Kosevich, A.M. On the theory of the de Haas–van Alphen effect for particles with an arbitrary dispersion law. *Dokl. Akad. Nauk SSSR [Proc. USSR Acad. Sci.]* **1954**, *96*, 963–966.
3. Yagi, R.; Iye, Y.; Osada, T.; Kagoshima, S. Semiclassical interpretation of the angular-dependent oscillatory magnetoresistance in quasi-two-dimensional systems. *J. Phys. Soc. Jpn.* **1990**, *59*, 3069–3072. [CrossRef]
4. Moses, P.; McKenzie, R.H. Comparison of coherent and weakly incoherent transport models for the interlayer magnetoresistance of layered Fermi liquids. *Phys. Rev. B* **1999**, *60*, 7998–8011. [CrossRef]
5. Kartsovnik, M.V. High magnetic fields: A tool for studying electronic properties of layered organic metals. *Chem. Rev.* **2004**, *104*, 5737–5782. [CrossRef] [PubMed]
6. Wosnitza, J. *Fermi Surfaces of Low-Dimensional Organic Metals and Superconductors*; Springer: Berlin/Heidelberg, Germany, 2013. [CrossRef]
7. Bergemann, C.; Julian, S.R.; Mackenzie, A.P.; NishiZaki, S.; Maeno, Y. Detailed topography of the Fermi surface of $Sr_2RuO_4$. *Phys. Rev. Lett.* **2000**, *84*, 2662–2665. [CrossRef] [PubMed]
8. Grigoriev, P.D. Angular dependence of the Fermi surface cross-section area and magnetoresistance in quasi-two-dimensional metals. *Phys. Rev. B* **2010**, *81*, 205122. [CrossRef]
9. Grigoriev, P.D. Weakly incoherent regime of interlayer conductivity in a magnetic field. *Phys. Rev. B* **2011**, *83*, 245129. [CrossRef]
10. Grigoriev, P.D.; Kartsovnik, M.V.; Biberacher, W. Magnetic-field-induced dimensional crossover in the organic metal $\alpha$-(BEDT-TTF)$_2$KHg(SCN)$_4$. *Phys. Rev. B* **2012**, *86*, 165125. [CrossRef]
11. Grigoriev, P.D. Longitudinal interlayer magnetoresistance in strongly anisotropic quasi-two-dimensional metals. *Phys. Rev. B* **2013**, *88*, 054415. [CrossRef]
12. Grigoriev, P.D.; Mogilyuk, T.I. Angular dependence of magnetoresistance in strongly anisotropic quasi-two-dimensional metals: Influence of Landau-level shape. *Phys. Rev. B* **2014**, *90*, 115138. [CrossRef]
13. Grigoriev, P.D.; Mogilyuk, T.I. False spin zeros in the angular dependence of magnetic quantum oscillations in quasi-two-dimensional metals. *Phys. Rev. B* **2017**, *95*, 195130. [CrossRef]
14. Kartsovnik, M.V.; Grigoriev, P.D.; Biberacher, W.; Kushch, N.D.; Wyder, P. Slow oscillations of magnetoresistance in quasi-two-dimensional metals. *Phys. Rev. Lett.* **2002**, *89*, 126802. [CrossRef] [PubMed]
15. Grigoriev, P.D. Theory of the Shubnikov–de Haas effect in quasi-two-dimensional metals. *Phys. Rev. B* **2003**, *67*, 144401. [CrossRef]
16. Grigoriev, P.D.; Ziman, T. Magnetic oscillations measure interlayer coupling in cuprate superconductors. *Phys. Rev. B* **2017**, *96*, 165110. [CrossRef]
17. Mogilyuk, T.I.; Grigoriev, P.D. Magnetic oscillations of in-plane conductivity in quasi-two-dimensional metals. *Phys. Rev. B* **2018**, *98*, 045118. [CrossRef]
18. Grigoriev, P.D.; Kartsovnik, M.V.; Biberacher, W.; Kushch, N.D.; Wyder, P. Anomalous beating phase of the oscillating interlayer magnetoresistance in layered metals. *Phys. Rev. B* **2002**, *65*, 060403. [CrossRef]
19. Schiller, M.; Schmidt, W.; Balthes, E.; Schweitzer, D.; Koo, H.-J.; Whangbo, M.H.; Heinen, I.; Klausa, T.; Kircher, P.; Strunz, W. Investigations of the Fermi surface of a new organic metal: (BEDT-TTF)$_4$[Ni(dto)$_2$]. *Europhys. Lett.* **2000**, *51*, 82. [CrossRef]
20. Weiss, H.; Kartsovnik, M.V.; Biberacher, W.; Balthes, E.; Jansen, A.G.M.; Kushch, N.D. Angle-dependent magnetoquantum oscillations in $\kappa$-(BEDT-TTF)$_2$Cu[N(CN)$_2$]Br. *Phys. Rev. B* **1999**, *60*, R16259–R16262. [CrossRef]
21. Kang, W.; Jo, Y.; Noh, D.-Y.; Son, K.-I.; Chung, O.-H. Appearance of beating in the Shubnikov–de Haas oscillations of the organic conductor $\kappa$-(BEDT-TTF)$_2$Cu(NCS)$_2$ under pressure. *J. Phys. Soc. Jpn.* **2010**, *79*, 044716. [CrossRef]
22. Krstovska, D. Quantum oscillations of the interlayer magnetothermopower in a Q2D organic conductor. *J. Phys. Soc. Jpn.* **2011**, *80*, 044701. [CrossRef]
23. Audouard, A.; Fortin, J.Y.; Vignolles, D.; Lyubovskii, R.B.; Drigo, L.; Shilov, G.V.; Duc, F.; Zhilyaeva, E.I.; Lyubovskaya, R.N.; Canadell, E. Non-Lifshitz–Kosevich field- and temperature-dependent amplitude of quantum oscillations in the quasi-two dimensional metal $\theta$-(ET)$_4$ZnBr$_4$(C$_6$H$_4$Cl$_2$). *J. Phys. Condens. Matter* **2015**, *27*, 315601. [CrossRef]
24. Arnold, F.; Naumann, M.; Rosner, H.; Kikugawa, N.; Graf, D.; Balicas, L.; Terashima, T.; Uji, S.; Takatsu, H.; Khim, S.; et al. Fermi surface of $PtCoO_2$ from quantum oscillations and electronic structure calculations. *Phys. Rev. B* **2020**, *101*, 195101. [CrossRef]
25. Oberbauer, S.; Erkenov, S.; Biberacher, W.; Kushch, N.D.; Gross, R.; Kartsovnik, M.V. Coherent heavy charge carriers in an organic conductor near the bandwidth-controlled Mott transition. *Phys. Rev. B* **2023**, *107*, 075139. [CrossRef]
26. Wang, J.-F.; Dong, Q.-X.; Huang, Y.-F.; Wang, Z.-S.; Guo, Z.-P.; Wang, Z.-J.; Ren, Z.-A.; Li, G.; Sun, P.-J.; Dai, X.; et al. Quantum oscillations in the magnetic Weyl semimetal NdAlSi arising from strong Weyl fermion–4$f$ electron exchange interaction. *Phys. Rev. B* **2023**, *108*, 024423. [CrossRef]
27. Xu, S.; Bao, C.; Guo, P.-J.; Wang, Y.-Y.; Yu, Q.-H.; Sun, L.-L.; Su, Y.; Liu, K.; Lu, Z.-Y.; Zhou, S.; et al. Interlayer quantum transport in Dirac semimetal $BaGa_2$. *Nat. Commun.* **2020**, *11*, 2370. [CrossRef]
28. Hornung, J.; Mishra, S.; Stirnat, J.; Raba, M.; Schwarze, B.V.; Klotz, J.; Aoki, D.; Wosnitza, J.; Helm, T.; Sheikin, I. Anomalous quantum oscillations of $CeCoIn_5$ in high magnetic fields. *Phys. Rev. B* **2021**, *104*, 235155. [CrossRef]
29. Zeng, X.-Y.; Dai, Z.-Y.; Xu, S.; Zhao, N.-N.; Wang, H.; Wang, X.-Y.; Lin, J.-F.; Gong, J.; Ma, X.-P.; Han, K.; et al. Quantum oscillations and weak anisotropic resistivity in the chiral fermion semimetal PdGa. *Phys. Rev. B* **2022**, *106*, 205120. [CrossRef]

30. Luo, X.; Ma, X.; Zhang, J.; Xing, Y.; Shen, A.; Ye, H.; Shen, S.; Peng, J.; Cao, S.; Dong, S.; et al. Investigation of de Haas–van Alphen and Shubnikov–de Haas quantum oscillations in $PrTe_3$. *Phys. Rev. B* **2024**, *109*, 035121. [CrossRef]
31. Daschner, M.; Grosche, F.M.; Liu, C.; Gudac, B.; Novak, M.; Kokanović, I. Probing the Fermi surface with quantum oscillation measurements in the Dirac semimetal $TaNiTe_5$. *arXiv* **2024**, arXiv:2403.12921. [CrossRef]
32. Leeb, V.; Polyudov, K.; Mashhadi, S.; Biswas, S.; Valentí, R.; Burghard, M.; Knolle, J. Anomalous quantum oscillations in a heterostructure of graphene on a proximate quantum spin liquid. *Phys. Rev. Lett.* **2021**, *126*, 097201. [CrossRef]
33. Alisultanov, Z.Z.; Abdullaev, G.O.; Grigoriev, P.D.; Demirov, N.A. Quantum oscillations of interlayer conductivity in a multilayer topological insulator. *J. Exp. Theor. Phys.* **2023**, *136*, 353–367. [CrossRef]
34. Abrikosov, A.A. *Fundamentals of the Theory of Metals*; North-Holland, Elsevier Science Publishers B.V.: Amsterdam, The Netherlands, 1988; Available online: https://archive.org/details/fundamentalsofth0000abri/ (accessed on 20 June 2024).
35. Ziman, J.M. *Principles of the Theory of Solids*; Cambridge University Press: Cambridge, UK, 1972. [CrossRef]
36. Wosnitza, J.; Wanka, S.; Hagel, J.; Löhneysen, H.v.; Qualls, J.S.; Brooks, J.S.; Balthes, E.; Schlueter, J.A.; Geiser, U.; Mohtasham, J.; et al. Field-induced metal–insulator transition in a two-dimensional organic superconductor. *Phys. Rev. Lett.* **2001**, *86*, 508–511. [CrossRef]
37. Laramee, B.; Ghimire, R.; Graf, D.; Martin, L.; Blundell, T.J.; Agosta, C.C. Superconductivity and Fermi surface studies of $\beta$"-$(BEDT\text{-}TTF)_2[(H_2O)(NH_4)_2Cr(C_2O_4)_3]$·8-crown-6. *Magnetochemistry* **2023**, *9*, 64. [CrossRef]
38. Champel, T.; Mineev, V.P. Magnetic quantum oscillations of the longitudinal conductivity $\sigma_{zz}$ in quasi-two-dimensional metals. *Phys. Rev. B* **2002**, *66*, 195111. [CrossRef]
39. Datta, B.; Adak, P.C.; Shi, L.-K.; Watanabe, K.; Taniguchi, T.; Song, J.C.W.; Deshmukh, M.M. Nontrivial quantum oscillation geometric phase shift in a trivial band. *Sci. Adv.* **2019**, *5*, eaax6550. [CrossRef] [PubMed]
40. Xu, X.; Kang, Z.; Chang, T.R.; Lin, H.; Bian, G.; Yuan, Z.; Qu, Z.; Zhang, J.; Jia, S. Quantum oscillations in the noncentrosymmetric superconductor and topological nodal-line semimetal $PbTaSe_2$. *Phys. Rev. B* **2019**, *99*, 104516. [CrossRef]
41. Zhao, W.; Wang, X. Berry phase in quantum oscillations of topological materials. *Adv. Phys. X* **2022**, *7*, 2064230. [CrossRef]
42. Nie, Y.; Tu, W.; Yang, Y.; Chen, Z.; Wang, Y.; Pan, S.; Mei, M.; Zhu, X.; Lu, W.; Ning, W.; et al. Quantum oscillations and nontrivial topological properties of layered metal $SrAg_4Sb_2$. *Appl. Phys. Lett.* **2023**, *123*, 163101. [CrossRef]
43. Sebastian, S.E.; Harrison, N.; Lonzarich, G.G. Towards resolution of the Fermi surface in underdoped high-$T_c$ superconductors. *Rep. Prog. Phys.* **2012**, *75*, 102501. [CrossRef] [PubMed]
44. Vignolle, B.; Vignolles, D.; Julien, M.H.; Proust, C. From quantum oscillations to charge order in high-$T_c$ copper oxides in high magnetic fields. *Comp. Rend. Phys.* **2013**, *14*, 39–52. [CrossRef]
45. Helm, T.; Kartsovnik, M.V.; Bartkowiak, M.; Bittner, N.; Lambacher, M.; Erb, A.; Wosnitza, J.; Gross, R. Evolution of the Fermi surface of the electron-doped high-temperature superconductor $Nd_{2-x}Ce_xCuO_4$ revealed by Shubnikov–de Haas oscillations. *Phys. Rev. Lett.* **2009**, *103*, 157002. [CrossRef] [PubMed]
46. Breznay, N.P.; Hayes, I.M.; Nair, N.L.; Helm, T.; Analytis, J.G.; McDonald, R.D.; Zhu, Z.; Krockenberger, Y.; Irie, H.; Yamamoto, H.; et al. Interplay of structure and charge order revealed by quantum oscillations in thin films of $Pr_2CuO_{4\pm\delta}$. *Phys. Rev. B* **2019**, *100*, 235111. [CrossRef]
47. Carrington, A. Quantum oscillation studies of the Fermi surface of iron-pnictide superconductors. *Rep. Prog. Phys.* **2011**, *74*, 124507. [CrossRef]
48. Coldea, A.I.; Braithwaite, D.; Carrington, A. Iron-based superconductors in high magnetic fields. *C. R. Phys.* **2013**, *14*, 94–105. [CrossRef]
49. Champel, T.; Mineev, V.P. de Haas–van Alphen effect in two- and quasi-two-dimensional metals and superconductors. *Philos. Mag. B* **2001**, *81*, 55–74. [CrossRef]
50. Grigoriev, P.D. The influence of the chemical potential oscillations on the de Haas-van Alphen effect in quasi-two-dimensional compounds. *J. Exp. Theor. Phys.* **2001**, *92*, 1090–1094. [CrossRef]
51. Balthes, E. Electron Correlations in the 2D Multilayer Organic Metal $\kappa$-$(BEDT\text{-}TTF)_2I_3$ in Magnetic Fields. Habilitation Thesis, University of Stuttgart: Stuttgart, Germany, 2004. [CrossRef]
52. Grigoriev, P.D.; Mogilyuk, T.I. Magnetic quantum oscillations of in-plane Hall conductivity and magnetoresistance tensor in quasi-two-dimensional metals. *arXiv* **2023**, arXiv:2312.07496. [CrossRef]
53. Fowler, M.; Prange, R.E. Electron-phonon renormalization effects in high magnetic fields. *Phys. Phys. Fiz.* **1965**, *1*, 315–328. [CrossRef]
54. Engelsberg, S.; Simpson, G. Influence of electron–phonon interactions on the de Haas–van Alphen effect. *Phys. Rev. B* **1970**, *2*, 1657–1665. [CrossRef]
55. Martin, G.W.; Maslov, D.L.; Reizer, M.Y. Quantum magneto-oscillations in a two-dimensional Fermi liquid. *Phys. Rev. B* **2003**, *68*, 241309. [CrossRef]
56. Adamov, Y.; Gornyi, I.V.; Mirlin, A.D. Interaction effects on magneto-oscillations in a two-dimensional electron gas. *Phys. Rev. B* **2006**, *73*, 045426. [CrossRef]
57. Chubukov, A.V.; Maslov, D.L. First–Matsubara–frequency rule in a Fermi liquid. I. Fermionic self-energy. *Phys. Rev. B* **2012**, *86*, 155136. [CrossRef]
58. Krstovska, D.; Choi, E.S.; Steven, E. Giant angular nernst effect in the organic metal $\alpha$-$(BEDT\text{-}TTF)_2KHg(SCN)_4$. *Magnetochemistry* **2023**, *9*, 27. [CrossRef]

59. Rehfuss, Z.; Broyles, C.; Graf, D.; Li, Y.; Tan, H.; Zhao, Z.; Liu, J.; Zhang, Y.; Dong, X.; Yang, H.; et al. Quantum oscillations in kagome metals $CsTi_3Bi_5$ and $RbTi_3Bi_5$. *Phys. Rev. Mater.* **2024**, *8*, 024003. [CrossRef]
60. Sakai, H.; Nakagawa, K.; Tsuruda, K.; Shiogai, J.; Akiba, K.; Tokunaga, M.; Kimura, S.; Awaji, S.; Tsukazaki, A.; Murakawa, H.; et al. Variation of Landau level splitting in the Fermi level controlled Dirac metals $(Eu, Gd)MnBi_2$. *Phys. Rev. B* **2023**, *108*, 115142. [CrossRef]
61. Zhang, W.; Wang, L.; Tsang, C.W.; Liu, X.; Xie, J.; Yu, W.C.; Lai, K.T.; Goh, S.K. Emergence of large quantum oscillation frequencies in thin flakes of the kagome superconductor $CsV_3Sb_5$. *Phys. Rev. B* **2022**, *106*, 195103. [CrossRef]